Hindawi
International Journal of Rotating Machinery
Volume 2022, Article ID 2006572, 15 pages
https://doi.org/10.1155/2022/2006572

Research Article

Dusting Hole Film Cooling Heat Transfer on a Transonic Turbine Blade Tip

Ward Manneschmidt,[1] Hallie Collopy,[1] Phillip Ligrani,[1] Kyle Goethals,[1] Matthew Cox,[1] Hongzhou Xu,[2] and Michael Fox[2]

[1]*University of Alabama in Huntsville, Huntsville, Alabama 35899, USA*
[2]*Solar Turbines Incorporated, San Diego, California 92186-5376, USA*

Correspondence should be addressed to Phillip Ligrani; pml0006@uah.edu

Received 21 May 2022; Revised 11 July 2022; Accepted 4 September 2022; Published 6 October 2022

Academic Editor: Terrence W. Simon

Investigated is a transonic turbine blade tip with a squealer rim and a squealer recess, with a single dusting film cooling hole contained within the leading edge region of the squealer recess. Data are provided for transonic flow conditions for a range of film cooling blowing ratios for two tip gap values, using a linear cascade, with no relative motion between the blade and the casing. Surface heat transfer characteristics are measured using the transient impulse-response measurement approach, employed with infrared thermography. Line-averaged adiabatic film cooling effectiveness values, for the 1.4 mm tip gap, are generally very small along the pressure side rim, with only small, locally increased values along the suction side rim. For the 0.8 mm tip gap, line-averaged adiabatic film cooling effectiveness values are generally somewhat higher along the pressure side rim and along the suction side rim. In general, effectiveness values for both tip gap values, for these locations, and for the recess region, increase as the blowing ratio increases. As the tip gap decreases from 1.4 mm to 0.8 mm, line-averaged adiabatic film cooling effectiveness generally increases on the rims and downstream regions of the recess, with increased magnitudes which are spread over larger spatial surface areas. For tip gaps of 0.8 mm and 1.4 mm, for regions where the line-averaged heat transfer coefficient ratio deviates significantly from 1.00, values generally decrease as the blowing ratio increases. Across every region of the blade, line-averaged heat transfer coefficient ratios either decrease or remain approximately invariant, as the tip gap value decreases from 1.4 mm to 0.8 mm.

1. Introduction

A transonic flow through a turbine blade tip gap is extremely complicated. This is because included within the tip gap are a variety of flow structural characteristics and phenomena, such as unsteady flow phenomena, normal and oblique shock waves, families of reflected shockwaves, augmented regions of high shear stress, regions of flow separation, regions of flow reattachment, three-dimensional secondary flows, and other flow effects. Parameters that affect such designs include the blade tip gap, number, positions, and orientations of film cooling holes, blade tip squealers, blowing ratio of the film cooling, and related parameters, as well as the presence of other complicated geometric arrangements on and near the blade tip. The present study considers a transonic turbine blade tip with a squealer rim and a squealer recess, with a single dusting film cooling hole (also referred to as a purge film cooling hole) contained within the upstream region of the squealer recess. Data are provided for transonic flow conditions over a set of film cooling conditions.

Previous investigations of dusting or purge film cooling on the tip of the turbine blade are rare. Only three studies are known which examine turbine blade tips with this type of film cooling arrangement in incompressible low speed flows [1–3]. Additional ten investigations consider dusting hole film cooling with subsonic compressible flows [4–13]. Only six studies are known which consider such film cooling arrangements with transonic flows around the turbine blade tip [14–19]. Of these investigations, only two of these

investigations [14, 16] provide experimental data for transonic conditions similar to actual engines.

Of investigations that consider low speed turbine blade tip heat transfer, Saxena and Ekkad [20] consider the effects of five different squealer geometries on heat transfer distributions on the blade tip and shroud using a steady-state liquid crystal technique. Results show that the location of the squealer rim has a significant effect on heat transfer magnitudes and that the full squealer has the lowest heat transfer distributions of the configurations investigated. In another subsonic study, Bang et al. [21] address the effects of unsteady wakes on the heat transfer of the turbine blade tip and shroud using the naphthalene sublimation measurement method. According to these investigators, the over tip leakage flow structure, including reattachment, vortices, and tip leakage vortex, is affected significantly by unsteady wakes when compared to arrangements without unsteady wakes.

For transonic conditions, Arisi et al. [14] present infrared thermography results and numerical prediction results for a linear cascade with ribbed squealer blades. Each blade includes a cooling hole near the leading edge and another near the center of the blade. Data are provided for Mach numbers of 0.85 and 1.00, with a blowing ratio of 1.0, and a 1 percent tip gap, relative to the blade span. Results show that flow reattachment in the cavity causes regions of high heat transfer. In addition, film cooling effectiveness decreases when the Mach number increases, with film cooling absent downstream of surface ribs. Ma et al. [16] discuss infrared thermography data from a linear cascade. Ma et al. [17] present the associated numerical prediction results. Six different film cooling hole arrangements on a squealer tip turbine blade are considered. The exit Mach number is 0.95, tip gap is 1.0 percent, relative to the blade span, and blowing ratio is 1.2. Significantly different surface heat transfer coefficient characteristics are observed on the squealer recess cavity floor, relative to the suction side rim. According to these investigators, the tip gap flow is greatly affected by the presence of film coolant injection. Numerically predicted vortex pairs are generated near each film cooling hole exit, where the vortices increase local heat transfer coefficients because of locally augmented secondary flows.

Kim et al. [15] present numerical simulation results for a rotating blade. A squealer turbine blade tip with three holes is utilized within the investigation. Data are given for a tip gap of 2 percent, relative to the blade span, with a rotor blade rotational speed of 17,000 rpm. According to these investigators, aerodynamics losses are decreased by changing the squealer recess depth, with simultaneous increases of film cooling effectiveness values. Tong et al. [18] present numerical prediction results for a rotating blade, which includes a turbine blade with a cutback squealer design, with two different film cooling hole arrangements. The turbine blade row rotational speed is 9,735 rpm, and squealer recess cavity depths are 1.875 percent, 2.5 percent, and 3.125 percent, relative to the blade span magnitude. According to these investigators, a larger number of holes near the blade-leading edge provides better film cooling effectiveness. Zhou [19] presents numerical prediction results for a turbine blade with a stationary casing wall and moving casing wall, where the velocity of the casing wall is set to be 0.35 of the inlet flow velocity. A turbine blade with a plain tip and a turbine blade with a squealer tip are utilized, where each contains coolant holes along the blade camber line. The tip gap is 1.9 percent, relative to the blade span, and coolant pressure ratio values of 0.9, 1.0, 1.1, and 1.2 are used. Local magnitudes of heat transfer coefficient increase, as the coolant pressure ratio becomes larger, an effect which is more pronounced with a plain blade tip. Also noted are relatively larger heat loads on the squealer blade tip when no film cooling is employed. With film cooling in use, surface heat loads along the squealer blade tip are approximately equivalent to heat loads along the surface of the flat blade tip. Also noted are increases of local film cooling effectiveness values, for the moving the casing wall, relative to the stationary casing wall arrangement.

The present study is unique and important because of the rarity of turbine blade tip studies with surface heat transfer measurements, dusting holes, squealer rims, a squealer recess, and transonic flow. The present investigation is also unique because a range of film cooling flow conditions is considered, with a film cooling density ratio of approximately 1.6. Data are provided for two tip gap values, with a single dusting film cooling hole contained within the leading edge region of the squealer recess. As mentioned, only two previous investigations [14, 16] are known to exist that describe transonic, surface heat transfer experimental results with dusting or purge holes located on the blade tip. Most other previous studies (which consider heat transfer characteristics from dusting hole film cooling) employ turbine blade tips, either in low-speed, incompressible flow [1–3], or in subsonic compressible flow [4–13]. Other recent investigations of transonic and subsonic tip gap flows, without heat transfer measurements, consider management of aerodynamic losses, aerothermodynamic characteristics, shock waves, and tip leakage vortices [22–26].

2. Facility and Research Approach

2.1. High-Speed Wind Tunnel. The high-speed wind tunnel facility utilized for the current study is a blow-down facility and is described by Sampson et al. [27] and by Collopy et al. [28]. Employed is a bar grid upstream of the test section entrance to produce a cascade inlet turbulence intensity magnitude of about 6.7 percent. The bar grid has an open area of 48 percent of the inlet area and is installed at the end of the nozzle that is upstream of the test section. The turbulence intensity is measured with a hot wire sensor that measures time-varying longitudinal velocity at the inlet of the test section. The time-averaged longitudinal velocity and longitudinal turbulence intensity are then determined from these measurements. Details of the associated procedures are provided by Chappell et al. [29]. The blow down experiment takes 3 seconds to start-up and then maintains steady-state flow conditions for about 3 seconds.

2.2. Linear Cascade. A diagram of the test section is displayed in Figure 1 with its relevant dimensions. Displayed are the positions of the monitored middle turbine blade,

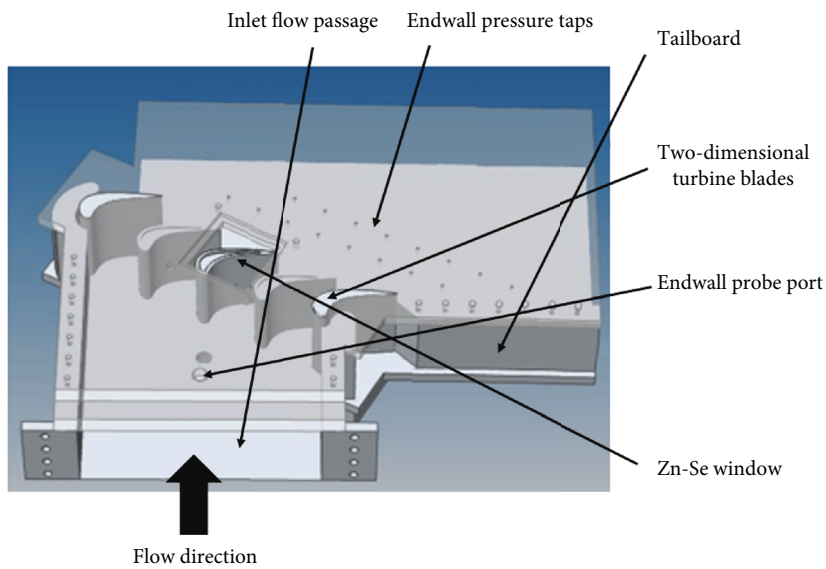

Figure 1: Schematic of linear cascade.

pitchwise bleed locations, and tailboard. Additionally, there are spanwise bleed slots at the entrance. A zinc-selenide window is positioned over the central turbine blade tip. Ports are positioned at the test section inlet to allow for probes to measure the mainstream static temperature, static pressure, and stagnation pressure. The same tip gap value and squealer rim and squealer recess arrangement are employed for all three of the middle blades within the cascade. The axial blade chord is 72.7 mm. The flow enters the cascade at an angle of 29°. The angle of the outlet is 62.3°. The blade pitch is 77.22 mm. Locations of downstream static pressure taps along the endwall are also shown within Figure 1. Measured surface static pressures at these locations demonstrate excellent cascade periodicity, achieved only with the lower tailboard and without the optional upper tailboard. Also note that, within the present linear cascade, no relative motion is present between the blade and the casing.

The estimated value of boundary layer thickness, relative to the casing surface, near the leading edge of each blade, is 4.0 mm or about 5.5 percent of the axial chord length C_x. The associated von Karman shape factor is estimated to be 1.31 to 1.34. At the cascade inlet, the flow static temperature, static pressure, stagnation pressure, sonic velocity, flow velocity, and Mach number are approximately 313.5 K, 172.5 kPa, 181.7 kPa, 354.9 m/sec, 95.8 m/sec, and 0.27, respectively. Near the cascade exit between blade wakes, static pressure, and Mach number are approximately 105.6 kPa and 0.93. The resulting Reynolds number, based upon C_x and inlet flow conditions, is 681,200.

Additional discussion of the cascade apparatus and flow conditions is provided by Collopy et al. [28].

2.3. Instrumented Film-Cooled Turbine Blade. Figures 2(a)–2(c) and 3(a) show specifics of the middle, monitored turbine blade. The span of the testing turbine blade is 85 mm. The span of the true blade is 120.91 mm. The present study investigated tip gaps of 0.8 mm and 1.4 mm. These distances correspond to 0.66 percent and 1.16 percent of the true blade span, respectively. The gap length of 1.4 mm corresponds to 1.9 percent of the axial chord, while the gap length of 0.8 mm corresponds to 1.1 percent of the axial chord. Note that squealer rims are employed to minimize the possibility of severe damage in the event of a tip rub. Presented in Figure 2(a) are the details of A1 film cooling configuration of the film-cooled blade. Presented in Figure 2(b) is the cut away view of the A1 instrumented blade. Lastly, presented in Figure 2(c) is the three-dimensional view of the A1 film-cooled blade.

Also visible in Figure 2(a) are the squealer recess, the squealer rim, and the single-dusting film cooling hole within the squealer recess zone. Note that the purposes of the squealer rims and squealer recess are to reduce the aerodynamic losses and surface heat loading along and downstream of the blade tip. The height of the squealer rim is 3.01 mm. The thickness of the rim changes along the perimeter of the turbine blade. The range of thickness variation for the squealer rim is from 2.07 mm to 4.17 mm. The single-dusting film cooling hole is located at $x = 0.206C_x$ from the leading edge of the blade. The diameter of the hole is 2.35 mm, with a perpendicular orientation (90 degree inclination angle) relative to the squealer recess surface. The length of the film cooling hole passage, along the centerline, is 0.877D. The present dusting hole film cooling configuration is denoted as the A1 configuration.

Additional details of the A1 film-cooled instrumented blade are presented in Figures 2(b) and 2(c). The carbon dioxide used as coolant is supplied through a plenum inside the monitored turbine blade. Also within the plenum are pressure ports, thermocouples to record the coolant temperature, and the entrance of the dusting film cooling hole.

2.4. Measurements of Temperature and Pressure. Surface static pressure is recorded around the perimeter of the blade at the 90 percent and 50 percent airfoil span location. The stagnation pressure is also measured slightly upstream of the sonic orifice (which is employed for measurements of

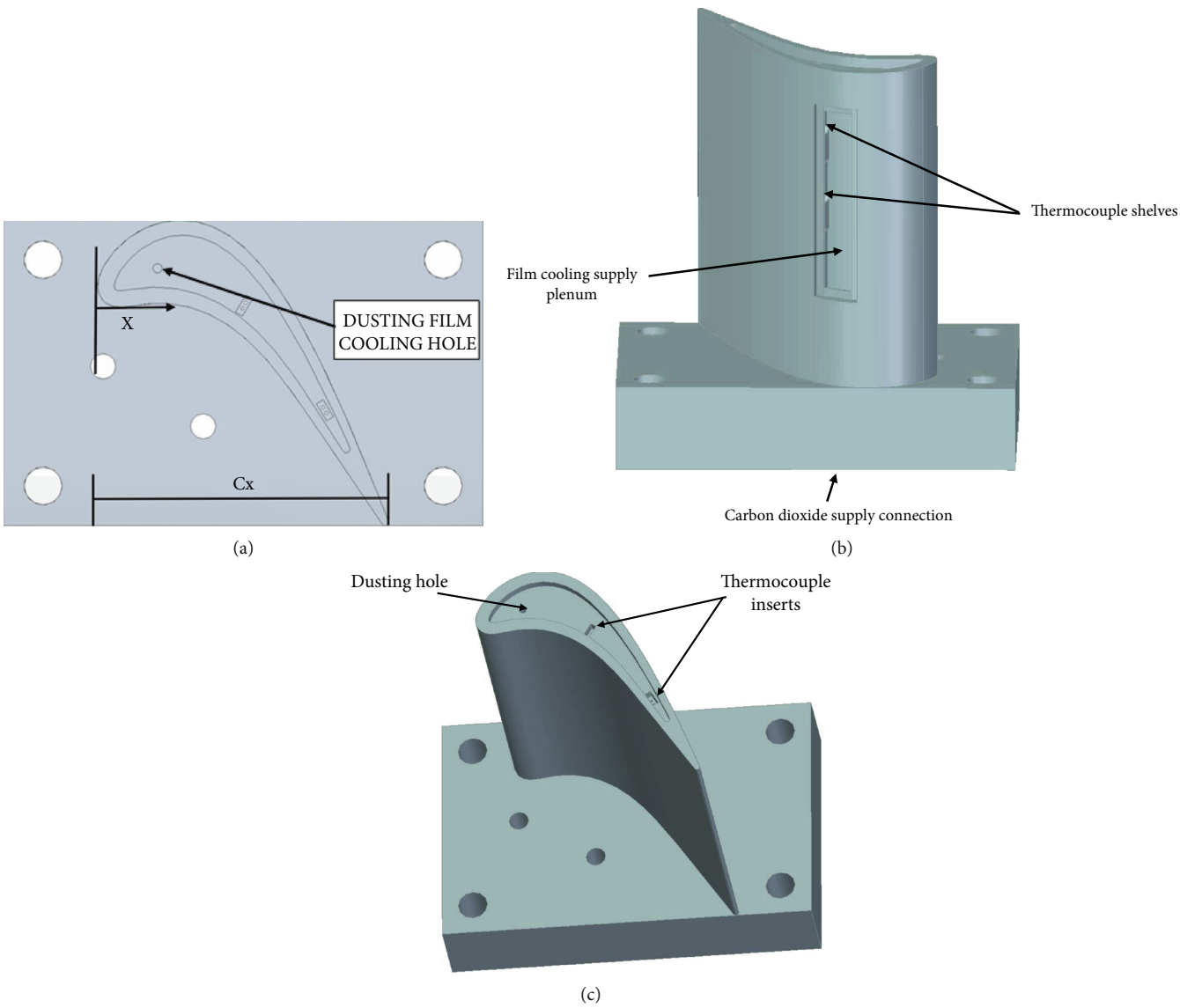

Figure 2: (a) Details of A1 film cooling configuration of the film-cooled blade. (b) Cut away view of the A1 instrumented blade. (c) Three dimensional view of the A1 film-cooled blade.

carbon dioxide coolant mass flow rates) and total pressure at two points in the instrumented blade internal plenum. A wall static pressure tap measures the mainstream flow static pressure at the entrance to the cascade, while a Kiel probe measures the stagnation pressure. All pressure measurements are taken with Honeywell digital pressure transducers. The response time for these pressure measurement systems is estimated to be from 0.05 to 0.10 seconds. For more details on these measurement systems, see Collopy et al. [28].

For details on the calibration of the pressure transducers, see Collopy et al. [28].

The air temperatures are recorded with two Omega Type T thermocouples at the cascade inlet. The response time of these thermocouples is approximately 0.050 seconds. Omega Type T thermocouples are used to measure the stagnation temperature inside the blade plenum and slightly upstream of the sonic orifice. Some more Omega Type T thermocouples are used to measure the surface temperature at several points on the surface of the blade tip. The temperature measurements from blade tip thermocouples are used for in-place calibration of the IR thermography camera. For this, four Type T thermocouples are used. The response time of these surface-mounted thermocouples is estimated to be from 0.005 to 0.010 seconds. Collopy et al. [28] provide additional details on the thermocouple measurement apparatus and procedures and in regard to thermocouple calibration.

2.5. Secondary Gas Supply. Carbon dioxide is selected to be the film coolant in order to match density ratios that exist within actual-operating gas turbine engines more closely. A specially constructed system is used to provide the film coolant for the instrumented blade. The system uses a sonic orifice to allow mass flow rate calculations to be performed and a copper tube heat exchanger to control the carbon dioxide

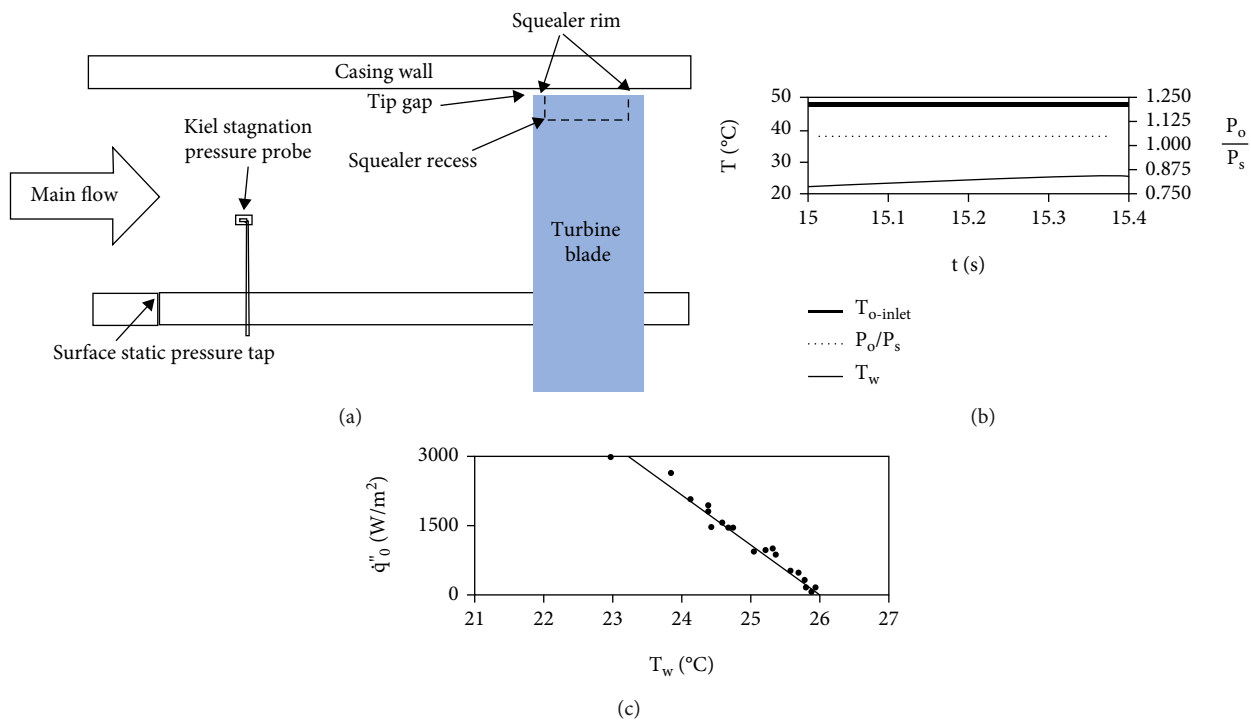

Figure 3: (a) Details of A1 film-cooled blade. (b) Variations of inlet stagnation temperature and ratio of total pressure to static pressure within the mainstream flow and variation of surface temperature at one location along the camber line within the squealer recess during a typical blowdown test for the dataset 2020-06-26-2025-c21. (c) Variation of local surface heat flux with surface temperature during a typical transient test at one location along the camber line within the squealer recess for the dataset 2020-06-26-2025-c21.

temperature. With this arrangement, the temperature of the carbon dioxide is 15°C to 20°C below ambient laboratory temperature when it is supplied to the blade [28].

2.6. Film Cooling Parameters. Relevant film cooling parameters are calculated from measurements of the mass flow rate, as well as the temperature and pressure of the carbon dioxide inside the turbine blade plenum. The calculated parameters include the static density and static temperature of the film coolant, and spatially averaged film coolant velocity at the dusting coolant hole exit. Additional calculated parameters for the exit plane of the dusting coolant hole include the momentum flux ratio, blowing ratio, discharge coefficient, and velocity ratio. Carbon dioxide is chosen for the film coolant to match turbine engine operating density ratios more accurately, as mentioned. Note that the procedures used to calculate the discharge coefficients are provided by Chappell et al. [29].

To calculate parameters for the film cooling, several local main stream flow parameters are needed from the film cooling hole exit location in the tip gap. To start the calculations, the first parameter needed is the local Mach number. The associated isentropic value is determined from squealer tip recess surface static pressure data. The dusting hole is positioned along the camber line at $x/C_x = 0.26$ within the squealer recess. The static pressure taps for measurement of local static pressure are located along the camber line at $x/C_x = 0.11$ and $x/C_x = 0.33$, also within the squealer recess. These static pressure measurements are then interpolated to obtain film cooling hole exit local flow conditions. Using the local Mach number, static pressure, and static temperature at the film cooling hole exit, the local sonic velocity and static density are calculated.

The calculated film cooling testing parameters for the current study are displayed in Table 1. Collopy et al. [28] provide details regarding determination of the associated film cooling parameters.

2.7. Surface Heat Transfer Measurements and Adiabatic Film Cooling Effectiveness. A transient measurement technique is employed to determine local, spatially resolved distributions of adiabatic surface temperature and local, spatially resolved distributions of surface heat transfer coefficients. A key device employed for these efforts is a FLIR Systems Inc. Infrared Camera, which operates at infrared wavelengths of 7.5 μm to 14.0 μm. The infrared camera is mounted to view and obtain squealer tip surface data from a normal viewing direction. The IR thermography camera measures surface temperature fluctuations, while recording blade tip images through a window made of zinc-selenide. Instrumented blade components are comprised of Somos WaterShed XC 11122 plastic. This material is employed because of its high tensile strength and thermal properties. Four thermocouples are located 0.41 mm beneath the surface of the turbine blade tip, which are used to calibrate the infrared camera during testing. The effect of this material thickness between the thermocouples and the blade surface are included in determinations of experimental uncertainties of measured heat

Table 1: Film cooling experimental conditions.

Dataset	Blowing ratio	Momentum flux ratio	Density ratio
1.4 mm tip gap			
1	0	0	0
2	0.64	0.27	1.52
3	1.18	0.89	1.57
4	1.58	1.55	1.61
5	2.11	2.65	1.68
6	2.49	3.58	1.73
7	2.94	4.85	1.78
0.8 mm tip gap			
8	0	0	0
9	0.81	0.43	1.53
10	1.51	1.44	1.59
11	2.01	2.46	1.65
12	2.86	4.61	1.77

transfer characteristics. Because the time interval for data processing is about 300 milliseconds, the conduction penetration depth is minimal during each transient test.

The camera has in situ calibration performed by referencing surface temperature measurements taken by Type T thermocouples. During a blow down test, the infrared camera acquires thermal signatures at a rate of 30 frames per second with a resolution of 998 × 750 pixels using the FLIR IR Research Software. Four thermocouples at different surface locations are employed for determination of infrared calibration equations in the form of greyscale variation with surface temperature. Results from these different thermocouples consistently give the same calibration equation, which is highly repeatable, as time varies and as multiple datasets are acquired. The impulse response method is used to calculate the surface heat flux [27]. The impulse response method uses an impulse response digital filter, along with a fast Fourier transform, to reconstruct the heat flux time history for each pixel location from the digitized time variation of surface temperature. The resulting data encompasses adiabatic wall temperature data and spatially resolved heat transfer coefficient. Collopy et al. [28] provide additional details on the associated procedures for calibrations and measurements.

The mainstream air supply is heated due to the work done by the compressor. As a result, at the start of each test, the mainstream temperature rises from 25°C to 45°C above ambient temperatures; this occurs over 1.2 to 1.3 seconds. The resulting conditions allow for the use of the transient impulse response method, such that the $T_{o-inlet}$ thermal transient is present, after the flow is fully established within the test section. As data are acquired, associated transonic flow conditions are steady state.

Shown in Figure 3(b) are variations of inlet stagnation temperature and ratio of total pressure to static pressure within the mainstream flow and variation of surface temperature at one location along the camber line within the squealer recess. These data are provided for the time period of a typical blowdown test for the dataset 2020-06-26-2025-c21. Figure 3(c) presents the fluctuation of local surface temperature with surface heat flux for the same position and for the same dataset. To determine such a time variation of surface heat flux, an impulse response method is used to analyze the change of surface temperature over time, along with turbine blade material properties, and the assumption of semi-infinite, one-dimensional thermal conduction. From data like the ones shown in Figure 3(c), the surface heat transfer coefficient is determined from the slope of the heat flux versus surface temperature distribution for each measurement location. The adiabatic wall temperature is then calculated at every measurement position as the intercept value of wall temperature associated with zero surface heat flux.

With the present approach, the surface heat flux is given as follows:

$$\dot{q}_0'' = h\,(T_{AW-FC} - T_W) \tag{1}$$

For details and explanation of the equation as well as the associated analysis and experimental procedures, see Collopy et al. [28].

The adiabatic film cooling effectiveness is determined using

$$\eta_{AD} = [T_{AW-NFC} - T_{AW-FC}]/[T_{AW-NFC} - T_{e-c}] \tag{2}$$

To see details and discussion of the equation, associated analytical, and experimental procedures, see Collopy et al. [28].

2.8. Uncertainty Analysis. The estimates for the testing uncertainty are for confidence levels of 95 percent and calculated following the steps described by Moffat [30]. The uncertainty for measured pressures is about ±0.8 kPa, and the uncertainty of thermocouple measured temperatures is typically about ±0.1°C. The uncertainty for the Mach number is ±1.5 percent. The experimental uncertainty of the blowing ratio is ±4.0 percent. The experimental uncertainty of the coolant mass flow rate is also approximately ±4.0 percent. The uncertainty for the adiabatic film cooling effectiveness is ±0.006 for a nominal value of 0.10, for values less than or equal to 0.12. For adiabatic film cooling effectiveness values greater than 0.12, the uncertainty for the adiabatic effectiveness is ±5.0 percent. The heat transfer coefficient, h, has an uncertainty of ±8.0 percent. The baseline heat transfer coefficient h_o is around ±120 W/m^{2}K for 2000 W/m^{2}K. Note that an important contributor to uncertainties of quantities measured using infrared thermography is identification of calibration thermocouple locations. Also note that uncertainty estimates account for any nonuniform initial temperature which may be present at the start of each transient test.

3. Blade Mach Number Distributions

Figure 4 shows the Mach number distributions along the perimeter of the central blade at the 50 percent and 90

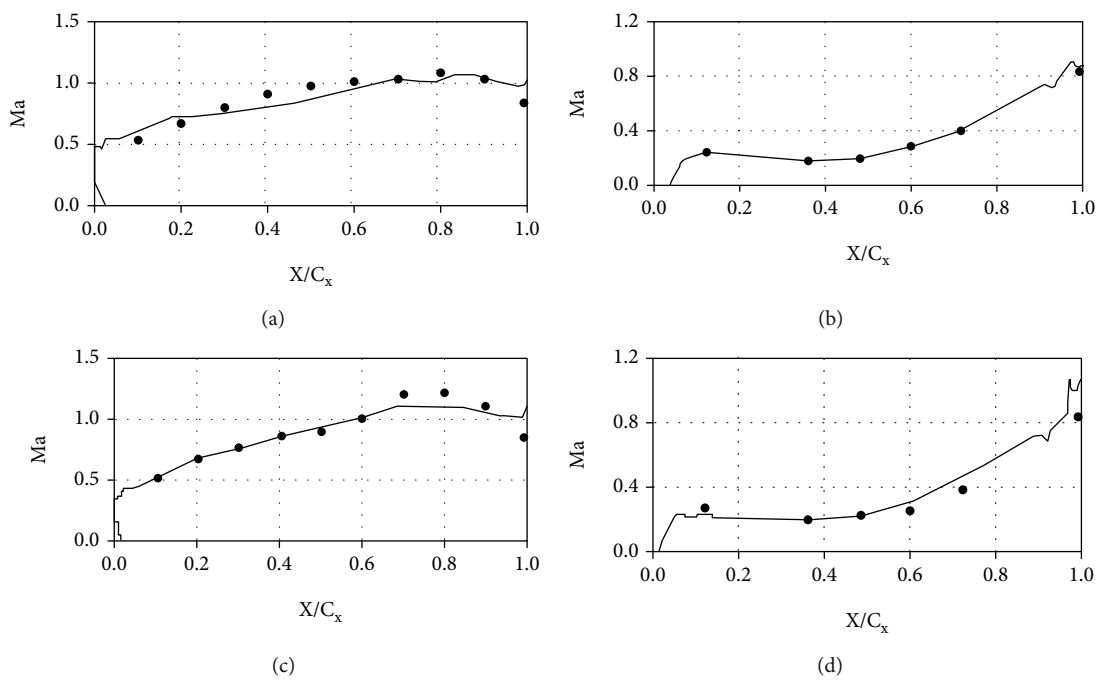

Figure 4: Central blade isentropic Mach number distributions for (a) suction surface at 50 percent span, (b) pressure surface at 50 percent span, (c) suction surface at 90 percent span, and (d) pressure surface at 90 percent span.

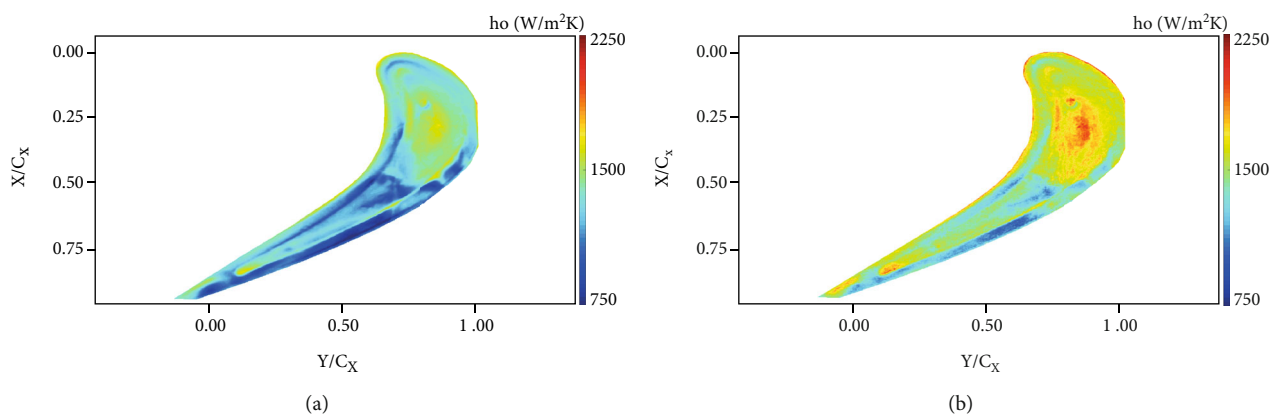

Figure 5: Baseline heat transfer coefficient ratio data along the squealer tip surface without film cooling. (a) Dataset 8, 0.8 mm tip gap. (b) Dataset 1, 1.4 mm tip gap.

percent spans on both the blade suction and pressure surfaces. Experimental data are plotted as circles, and the lines are RANS numerical predictions. The data shows that along the suction surface of the blade, the flow accelerates from subsonic to supersonic flow before reaching the end of the blade. The maximum Mach numbers achieved by the flow are around 1.1 and 1.25, for the 50 percent and 90 percent span locations, respectively. The data shows that along the pressure surface, despite the acceleration as the flow advects downstream, the flow remains subsonic.

4. Local, Spatially Resolved Surface Heat Transfer Coefficient Data Distributions

Spatially resolved baseline heat transfer coefficient data along the squealer tip surface, without film cooling, are given in Figures 5(a) and 5(b) for tip gaps of 0.8 mm and 1.4 mm, respectively. Except for the absence of film cooling, the present baseline results are obtained for the same experimental conditions which are employed when film cooling is included. The distributions match the data presented by Virdi et al. [31]. For discussion of baseline heat transfer distributions, see Collopy et al. [28].

5. Local, Spatially Resolved Blade Surface Adiabatic Film Cooling Effectiveness Distributions

Figures 6(a) and 6(b) present local distributions of adiabatic film cooling effectiveness on the turbine blade tip surface with A1 film cooling for tip gaps of 0.8 mm and 1.4 mm, with BR = 1.51 and BR = 1.58, respectively. Also included

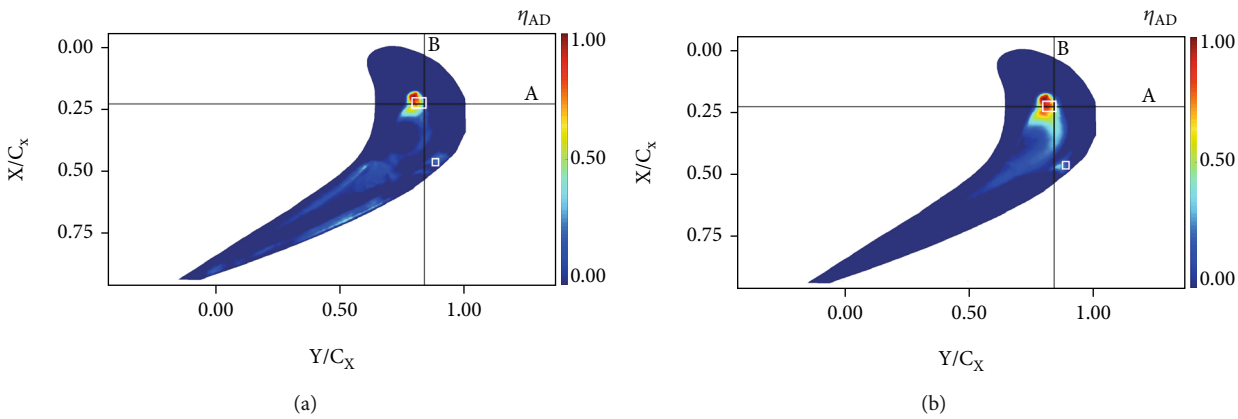

Figure 6: Locations A and B as well as regions for area averaging presented with respect to adiabatic film cooling effectiveness distribution. (a) Dataset 10, 0.8 mm tip gap, BR = 1.51. (b) Dataset 4, 1.4 mm tip gap, BR = 1.58.

within these figures are locations of lines A and B and regions for determination of area-averaged adiabatic film cooling effectiveness values. Note that effectiveness is locally increased at the A1 film cooling hole exit location in both figures, where values are in the vicinity of 1.0. Also note that local effectiveness magnitudes are strongly tied to the concentration amount of film coolant near and adjacent to the blade tip surface. Line locations A and B are selected to provide additional information regarding local data variations. In particular, the locations of lines A and B are selected to evaluate film cooling effectiveness and heat transfer coefficient ratio behavior near to and downstream of the dusting hole. Line location B is also selected to evaluate characteristics along the suction side rim.

The data within Figures 6(a) and 6(b) provide evidence that the coolant is detaching near the dusting hole exit and reattaching further downstream. The associated separation of coolant from the surface appears to be more pronounced for the 0.8 mm tip gap. Such characteristics are tied to local effectiveness increases, which are often present at locations immediately and then further downstream within the squealer recess region, as well as along the suction side and pressure side rim surfaces at locations of film coolant accumulation. Associated values of the effectiveness along the pressure and suction side rim can be as high as 0.4 to 0.45. With the 1.4 mm tip gap, effectiveness distributions indicate that, after the coolant exits the dusting hole, it flows along the recess surface for only a short distance before being advected out of the recess volume. The associated outflow is evidenced by small areas of elevated effectiveness values which are present on the suction side rim and by effectiveness readings in the vicinity of zero, within the farthest downstream portions of the squealer recess.

Local variations of adiabatic film cooling effectiveness along lines A and B are presented in Figures 7(a) and 7(b), respectively. These data are provided for both tip gap values for different blowing ratios. Note that vertical lines within Figures 7(a) and 7(b) denote the boundaries of the suction side squealer rim and the pressure side squealer rim.

Figure 7(a) shows values for line A, which are as high as about 0.90 within the recess region for Y/C_X values of 0.75–0.85. Here, values generally decrease as the blowing ratio increases. Except for the lowest blowing ratio, the film cooling effectiveness decreases as the tip gap decreases. This indicates that the coolant lift-off effect is more pronounced in the smaller tip gap near the film cooling dusting hole. Figure 7(b) shows that adiabatic effectiveness data values, along line B, are increased substantially within the recess region in the vicinity of X/C_X of 0.25. Here, effectiveness magnitudes usually decline as blowing ratio rises. Within the recess region, values for the 0.8 mm tip gap are much lower, which provides additional evidence that coolant lift-off is more pronounced for the smaller tip gap. Along the suction side rim portion of line B, effectiveness values are nonzero only for the 0.8 mm tip gap. The differences in film cooling effectiveness distributions over the tip can be attributed to a change in the flow structure of the over tip leakage flow with changes in the tip gap. Although the smaller tip gives lower values of adiabatic film cooling effectiveness and experiences more pronounced lift-off, this behavior does not necessarily equate to increased local heat transfer coefficients. In general, local advection through the tip gap has reduced velocities for the 0.8 mm tip gap, which results in lower local heat transfer coefficients.

6. Local, Spatially Resolved Surface Heat Transfer Coefficient Ratio Distributions

Figures 8(a) and 8(b) present local distributions of the heat transfer coefficient ratio on the turbine blade tip surface with A1 film cooling for tip gaps of 0.8 mm and 1.4 mm, with BR = 1.51 and BR = 1.58, respectively. Also included within these figures are locations of lines A and B and regions for determination of area-averaged heat transfer coefficient ratio values. Note that values of the heat transfer coefficient ratio within these figures are approximately equal to one away from film cooling trajectory locations.

Figures 8(a) and 8(b) show that heat transfer coefficient ratio distributions for the two tip gaps are qualitatively and quantitatively similar. Also evident are relatively high heat transfer coefficient ratios near the exit of the film cooling

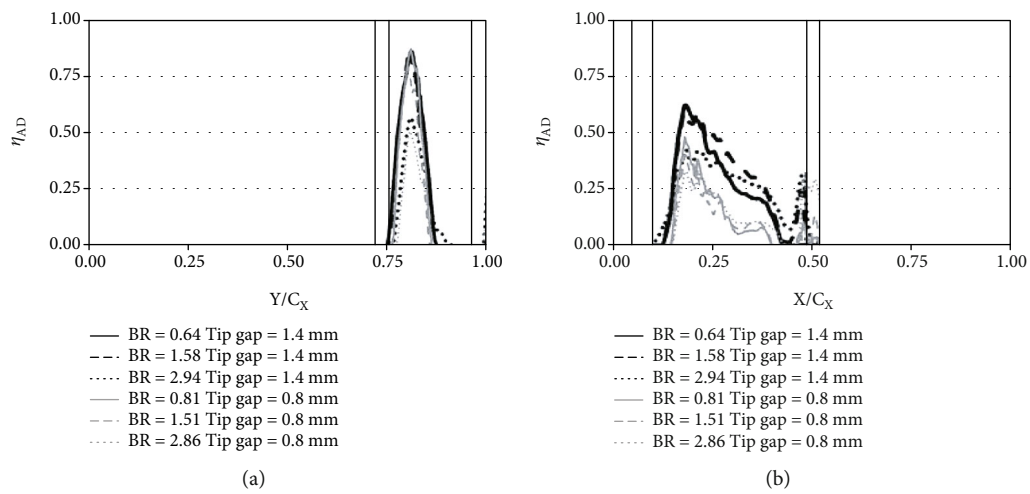

Figure 7: Local adiabatic film cooling effectiveness distributions for the A1 blade for different tip gaps and blowing ratios. (a) Along line A. (b) Along line B.

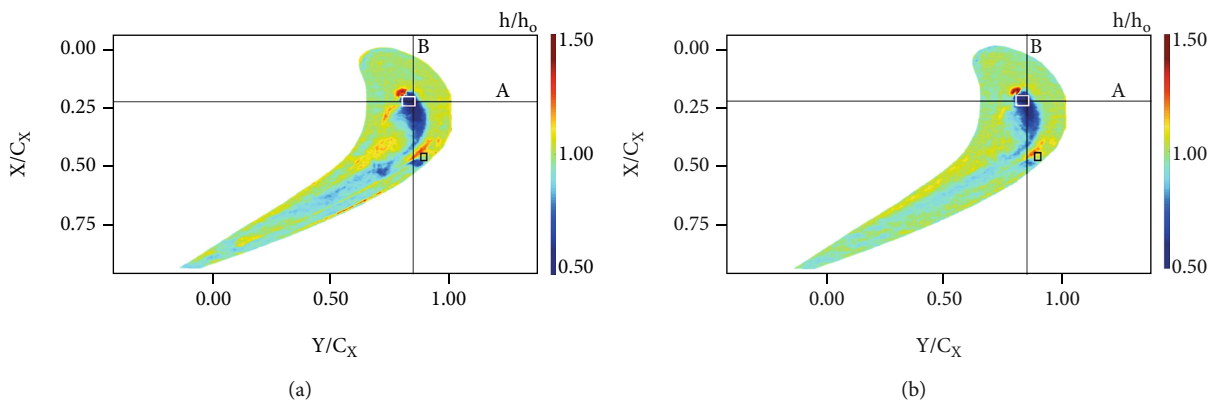

Figure 8: Locations A and B as well as regions for area averaging presented with respect to heat transfer coefficient ratio distribution, with film cooling. (a) Dataset 10, 0.8 mm tip gap, BR = 1.51. (b) Dataset 4, 1.4 mm tip gap, BR = 1.58.

hole, with much lower values along downstream film trajectory paths, within the recess region. Such local coefficient decreases are believed to be due to locally lower magnitudes of turbulence transport. Regions with heat transfer coefficient ratios less than one, where the film cooling effectiveness is relatively low, are caused by detachment of film concentrations from the squealer tip surface.

Local heat transfer coefficient ratio variations along lines A and B are presented in Figures 9(a) and 9(b), respectively. These data are provided for both tip gap values for different blowing ratios. Note that vertical lines within Figures 9(a) and 9(b) denote the boundaries of the suction side squealer rim and the pressure side squealer rim.

Figure 9(a) shows significant localized decreases of local heat transfer coefficient ratios near Y/C_X values of 0.85, with minimum values ranging from 0.35 to 0.85 as the blowing ratio is changed. Here, local ratios generally decrease as the tip gap decreases. Local ratio values also often decrease as the blowing ratio increases, which provides additional evidence that coolant concentrations are either partially or completely lifting off from the squealer recess surface. Such phenomena are also responsible for the data trends shown along line B in Figure 9(b), where local heat transfer coefficient ratios are generally less than 1.0 within the recess region. Here, local ratio values also often decrease as the blowing ratio BR increases. If the blowing ratio is approximately constant, local ratio values within Figure 9(b) generally decrease as the tip gap decreases for each X/C_x location within the recess region.

Within Figures 6, 7, 8, and 9, locations of the altered heat transfer coefficient ratio, which are different from one, correspond with locations where the adiabatic film cooling effectiveness is nonzero. However, in some cases, altered heat transfer coefficient ratios are associated with very low values of film effectiveness, which are near zero. For these situations, only minimal coolant is present next to the blade tip surface, even though larger accumulations are often present in outer parts of the boundary layers, which then alter local turbulent transport, as well as local heat transfer coefficient magnitudes.

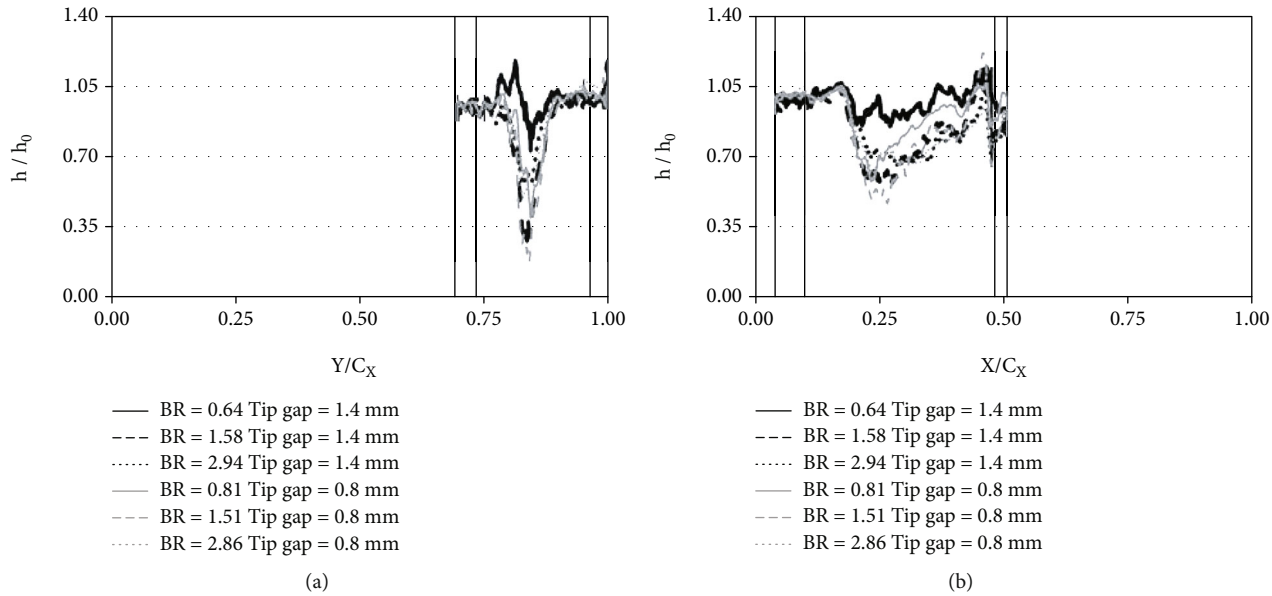

Figure 9: Local heat transfer coefficient ratio distributions for the A1 blade for different tip gaps and blowing ratios. (a) Along line A. (b) Along line B.

7. Line-Averaged Data Analysis Procedures

An example of the line-averaging layout is shown in Figure 10. For discussion and explanation of the line averaging software code and procedures, see Collopy et al. [28].

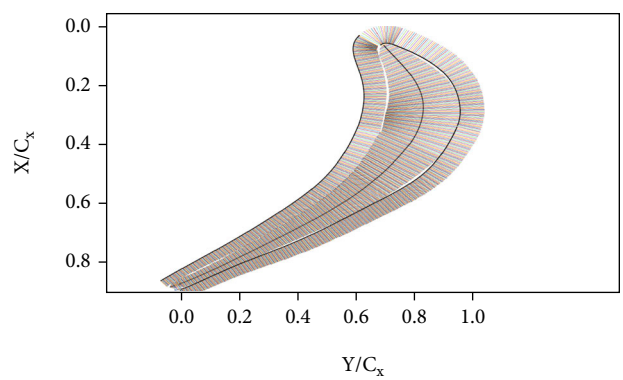

Figure 10: Locations of polynomial equations and regions for line averaging, along the squealer blade tip surface, for the pressure side rim, the squealer recess region, and the suction side rim.

8. Line-Averaged Blade Surface Adiabatic Film Cooling Effectiveness Distributions

Figures 11(a)–11(c) present line-averaged adiabatic film cooling effectiveness fluctuations on the pressure side rim, squealer recess region, and suction side rim, respectively. The presented data are for a tip gap of 0.8 mm with blowing ratios BR of 0.81, 1.51, and 2.86 and for a tip gap of 1.4 mm with blowing ratios BR of 0.64, andd1.58.

Data within Figure 11(a) show that adiabatic film cooling effectiveness values for three blowing ratios are zero or are very near to zero, along the pressure side rim for the 1.4 mm tip gap. With a tip gap of 0.8 mm, line-averaged effectiveness data generally increase as the blowing ratio increases at particular S/S_o values (as the tip gap value is constant). Figure 11(c) shows that adiabatic film cooling effectiveness data along the suction side rim are near zero until S/S_o becomes greater than 0.30. For S/S_o from 0.30 to 0.45, line-averaged effectiveness values generally increase as the blowing ratio increases (as the tip gap is constant) and generally increase as the tip gap decreases (while the blowing ratio is constant). For S/S_o greater than 0.55, effectiveness values are near zero for the 1.4 mm tip gap. With a tip gap of 0.8 mm, line-averaged effectiveness data for S/S_o greater than 0.55 generally increase as the blowing ratio increases (as the tip gap is constant).

Line-averaged adiabatic film cooling effectiveness data along the recess region in Figure 11(b) show local maxima near S/S_o near 0.15 due to the presence of the dusting film cooling hole exit. Here, effectiveness values generally increase as the blowing ratio decreases (as the tip gap is constant). Farther downstream, for S/S_o from 0.40 to 0.70, the opposite trend with a blowing ratio is generally apparent (as the tip gap is constant), such that effectiveness values generally increase as the tip gap decreases (as the blowing ratio is constant).

In general, the effectiveness results in Figures 11(a)–11(c) show that, with the 0.8 mm tip gap, effectiveness variations provide evidence that coolant separates from recess region surfaces in greater amounts, with reattachment further downstream, in comparison to the 1.4 mm tip gap. Effectiveness variations also provide evidence that coolant with the 0.8 mm tip gap is present in greater concentrations near squealer rim surfaces, relative to the 1.4 mm tip gap arrangement, especially for S/S_o numbers larger than 0.40

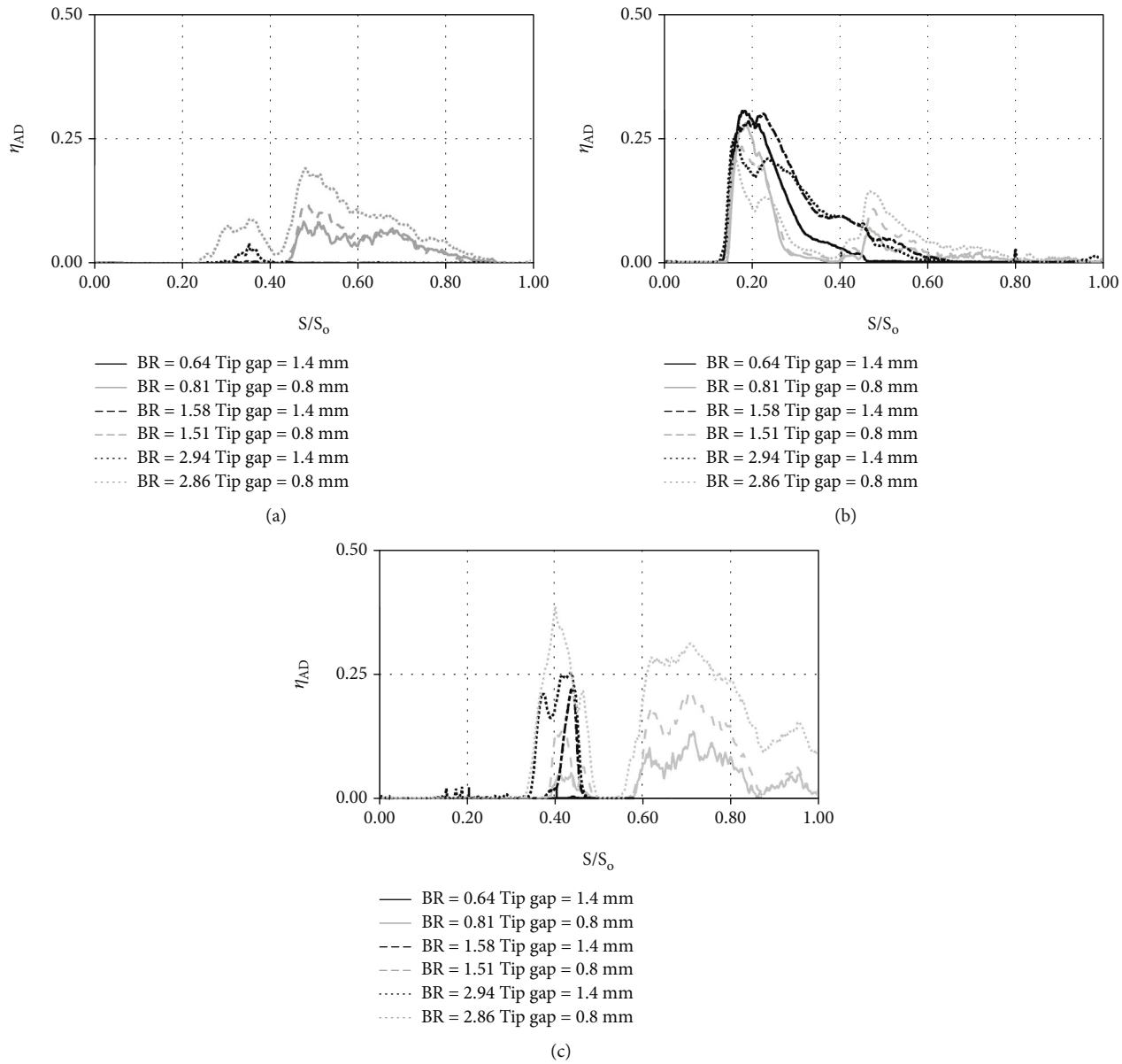

Figure 11: Line-averaged adiabatic film cooling effectiveness along for A1 blade film cooling for different blowing ratios and tip gaps. (a) Along the pressure side rim. (b) Along the squealer recess region. (c) Along the suction side rim.

to 0.55. The general trends shown in Figures 11 and 12 are consistent with Narzary et al. [32], who employ a turbine blade with a suction rim with tip gaps ranging from 0.87 percent to 2.3 percent of the blade span. The present date are also in agreement with results from Ullah et al. [33] in regard to film cooling effectiveness increases as the blowing ratio becomes larger. These investigators utilize a flat tip blade and consider experimental conditions with a large range of different density ratios.

9. Line-Averaged Blade Surface Heat Transfer Coefficient Ratio Distributions

Figures 12(a)–12(c) present line-averaged heat transfer coefficient ratio deviations on the pressure side rim, squealer recess region, and suction side rim, respectively. The presented data are for a tip gap of 0.8 mm with blowing ratios (BR) of 0.81, 1.51, and 2.86 and for a tip gap of 1.4 mm with blowing ratios BR of 0.64 and 1.58.

Figure 12(a) displays that heat transfer coefficient ratio data along the pressure side rim have almost no variation with the blowing ratio or tip gap until S/S_o becomes greater than 0.40. For S/S_o numbers larger than 0.40, values generally decrease as the blowing ratio increases (as the tip gap value is constant), such that values also generally decrease as the tip gap decreases (as the blowing ratio is approximately constant). Figure 12(c) shows that heat transfer coefficient ratio values on the suction side rim have almost no variation with the blowing ratio or tip gap until S/S_o becomes greater than 0.35 to 0.40. As S/S_o increases further, data for each blowing ratio and tip gap

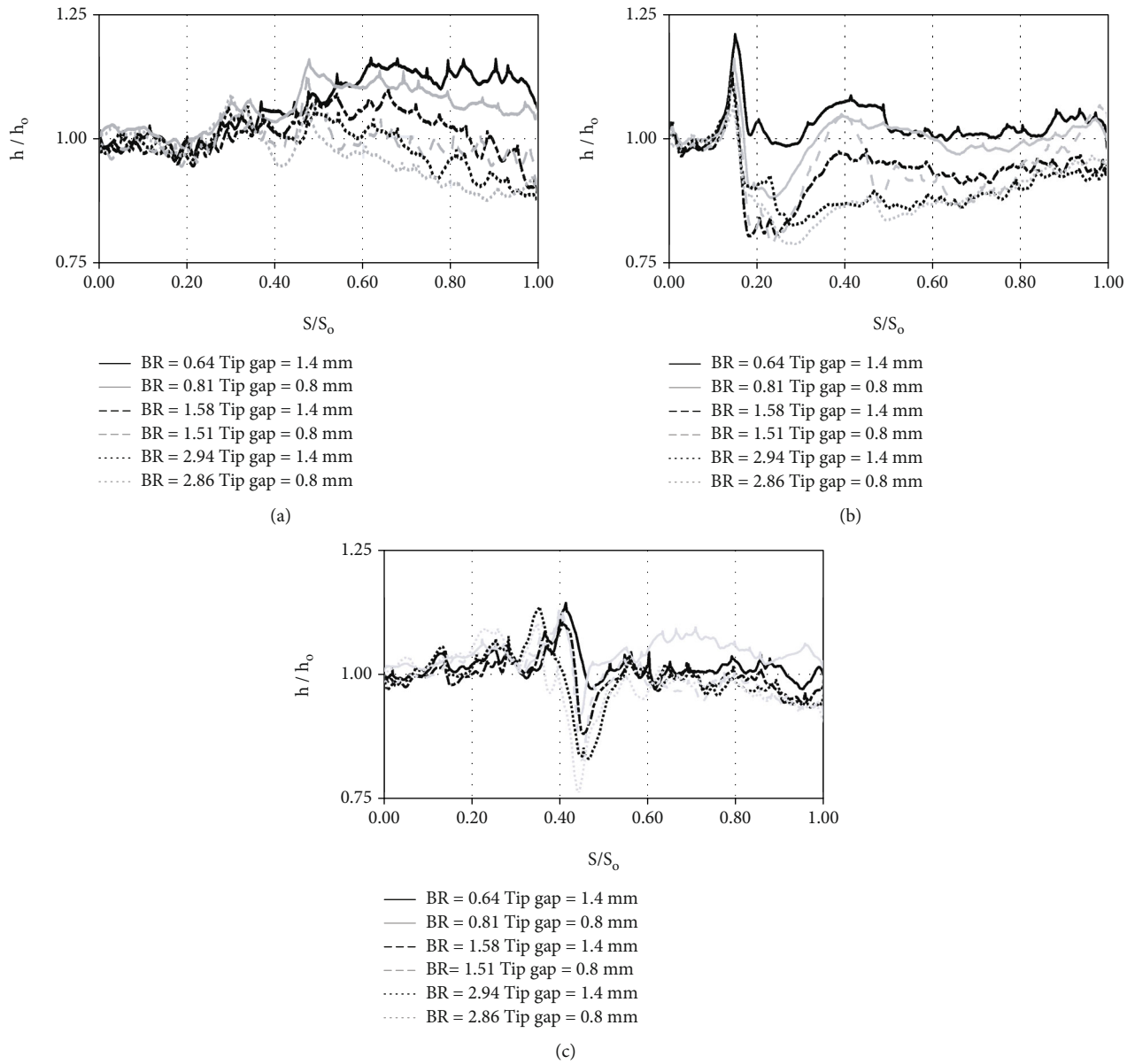

Figure 12: Line-averaged heat transfer coefficient ratio along for A1 blade film cooling for different blowing ratios and tip gaps. (a) Along the pressure side rim. (b) Along the squealer recess region. (c) Along the suction side rim.

generally first show a local maximum value, followed by a local minimum value. For larger S/S_o magnitudes, values generally decrease as the tip gap decreases (as the blowing ratio is approximately constant) and generally decrease as the blowing ratio increases (as the tip gap is constant).

Figure 12(b) shows heat transfer coefficient ratio variations as S/S_o increases, along the squealer recess region. Each dataset for particular values of the tip gap and blowing ratio shows a local maximum S/S_o near to 0.15, wherein ratios generally decrease as the blowing ratio becomes larger. These locally augmented heat transfer coefficients are believed to be due to intense secondary flows within a horseshoe-shaped vortex, which forms around each film cooling jet. Ratios then show a significant decrease as S/S_o becomes larger than 0.15, when values generally show almost no variation with a tip gap magnitude (as blowing ratio is approximately constant) but generally a decrease as the blowing ratio is increased for particular S/S_o values (and the tip gap is constant). Within Figure 12(b), heat transfer coefficient ratio differences for the tip gaps, within the minima value region, are most likely because coolant lift-off is more significant for the 0.8 mm tip gap, especially at lower blowing ratios.

10. Area-Averaged Blade Surface Adiabatic Film Cooling Effectiveness and Heat Transfer Coefficient Ratio Distributions

Figures 13(a) and 13(b) show area-averaged adiabatic film cooling effectiveness and heat transfer coefficient ratio

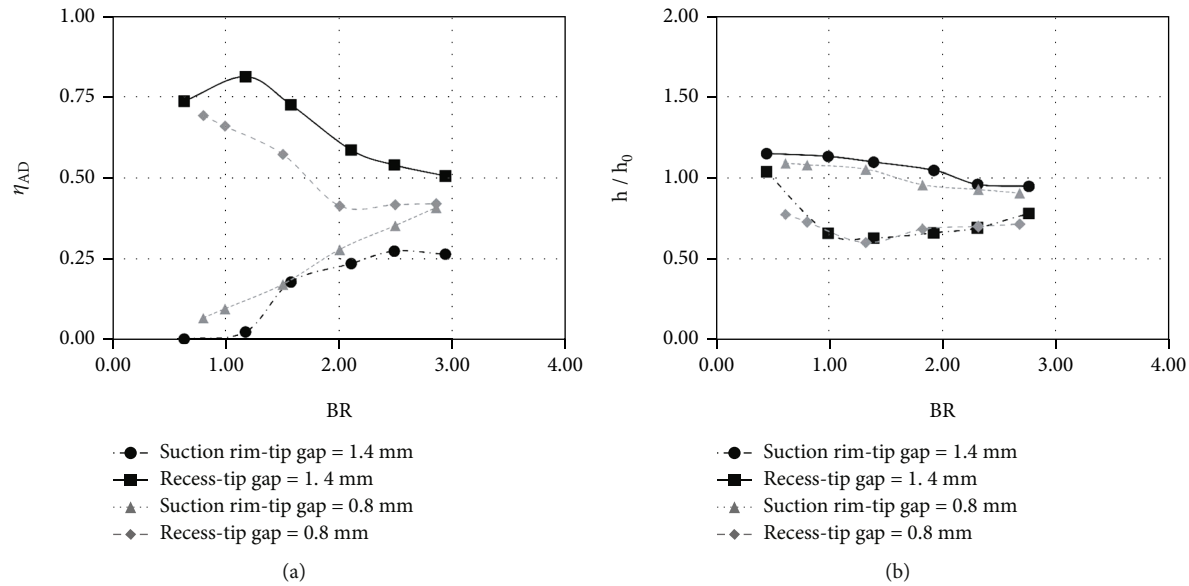

Figure 13: Area-averaged data variation for the A1 blade film cooling for different blowing ratios and tip gaps. (a) Adiabatic film cooling effectiveness. (b) Heat transfer coefficient ratio.

variations, respectively, with a blowing ratio for both tip gaps. Figures 6 and 8 show the locations for area-average determinations for tip gaps of both 1.4 millimeters and 0.8 millimeters.

Figure 13(a) shows that adiabatic film cooling effectiveness along the suction side rim increase as the blowing ratio increases (as the tip gap is constant) for both tip gap values. Generally, values for the 0.8 mm tip gap are larger for blowing ratios greater than 1.50. Figure 13(a) also shows that area-averaged adiabatic film cooling effectiveness values along the recess region generally decrease as the blowing ratio increases. Here, data for the 0.8 mm tip gap are consistently lower than numbers shown by the 1.4 mm tip gap, for each BR value considered. Such behavior is a consequence of significant separations of coolant concentrations from recess region surfaces, which changes with the tip gap magnitude.

Figure 13(b) shows that heat transfer coefficient ratios along the suction side rim decrease slightly as the blowing ratio increases, with 0.8 mm data slightly lower than the 1.4 mm date for each blowing ratio value. Values within the recess region are in approximate agreement for both tip gaps. In both cases, area-averaged heat transfer coefficient ratios decrease as the blowing ratio increases, for BR values up to 1.5. For higher BR values, area-averaged heat transfer coefficient ratios increase slowly as the blowing ratio increases from 1.5. Such characteristics are related to complex alterations of turbulent transport and flow mixing within the film-cooled boundary layers, as the tip gap and blowing ratio are altered.

Note that the values in Figure 13 are substantially higher than the line-averaged data values within Figures 11 and 12. This is because the area-averaged values are locally determined and do not cover the same surface regions employed to determine the line-averaged results shown in Figures 11 and 12.

11. Summary and Conclusions

Investigated is a transonic turbine blade tip with a squealer rim and a squealer recess, with a single dusting film cooling hole contained within the leading edge region of the squealer recess. Data are presented for transonic flow conditions for a range of film cooling blowing ratios for two tip gap values. Spatially resolved distributions of surface adiabatic film cooling effectiveness and surface heat transfer coefficients are provided for different film cooling flow conditions. The present study is unique and important because of the rarity of turbine blade tip studies with surface heat transfer measurements, dusting holes, squealer rims, and transonic flow.

Line-averaged adiabatic film cooling effectiveness values for the 1.4 mm tip gap are generally very small on the pressure side rim, with a small, locally increased values along the suction side rim. For the 0.8 mm tip gap, line-averaged adiabatic film cooling effectiveness values are generally somewhat higher along the pressure side rim and along the suction side rim. In general, effectiveness values for both tip gap values, for these locations, and for the recess region, increase as the blowing ratio increases. One important exception to this trend is apparent near the dusting hole within the recess region, where line-averaged adiabatic film cooling effectiveness values decrease as the blowing ratio increases.

For tip gaps of 0.8 mm and 1.4 mm, for regions where the line-averaged heat transfer coefficient ratio deviates significantly from 1.00, values generally decrease as the blowing ratio increases. One exception to this trend is apparent within the recess region, near the dusting hole exit location in the vicinity of S/S_o equal to 0.20, where the lowest heat transfer coefficient ratio value is associated with an intermediate magnitude of the blowing ratio. The smaller tip gap arrangement generally gives lower or slightly lower heat transfer coefficient ratios, compared to the 1.4 mm tip gap configuration, when compared at the same blade tip location and same blowing ratio. Because

improved thermal protection is associated with lower local heat transfer coefficients, the 0.8 mm tip gap consistently provides more favorable thermal protection, overall, relative to the 1.4 mm tip gap configuration.

NOMENCLATURE

BR: Film cooling blowing ratio
c: Sonic velocity
C_d: Discharge coefficient
C_x: Axial chord length
D: Film cooling hole diameter
DR: Density ratio
h: Isoenergetic heat transfer coefficient
h_o: Baseline heat transfer coefficient
I: Momentum flux ratio
$\dot{m}_c$: Mass flow rate of the carbon dioxide film coolant
Ma: Mach number
P_s: Static pressure
P_T: Stagnation pressure
$\dot{q}_0''$: Wall heat flux
R_c: Gas constant for carbon dioxide
S: Coordinate along the line represented by polynomial equation
S_o: Coordinate along the line represented by polynomial equation from blade leading edge to trailing edge
T_{AW}: Surface adiabatic wall temperature
T_{o-c}: Coolant stagnation temperature
$T_{o-inlet}$: Inlet cascade stagnation temperature
T_s: Static temperature
T_t: Stagnation temperature
T_W: Wall temperature
v: Flow velocity
VR: Velocity ratio
x: Axial coordinate
X: Axial coordinate
y: Pitch coordinate
Y: Pitch coordinate
γ_c: Ratio of specific heats for carbon dioxide
ρ: Static density
η_{AD}: Adiabatic film cooling effectiveness.

Subscripts

Avg: Spatially averaged value
c: Film cooling value or coolant value
e: Film cooling hole exit value
FC: Film cooling value
ideal: Ideal isentropic value
local: Local flow value at exits of film cooling holes
ms: Main flow value
NFC: No film cooling value
s: Static value.

Data Availability

All data presented within the paper are available in a digital format upon request.

Conflicts of Interest

The authors declare that they have no conflicts of interest.

Acknowledgments

The research effort was funded and supported by the Solar Turbines Incorporated of San Diego, California, USA.

References

[1] J. Y. Jeong, W. Kim, J. S. Kwak, and J. S. Park, "Heat transfer coefficient and film cooling effectiveness on the partial cavity tip of a gas turbine blade," *Journal of Turbomachinery*, vol. 141, no. 7, pp. 1–9, 2019.

[2] P. J. Newton, G. D. Lock, S. K. Krishnababu et al., "Aerothermal investigations of tip leakage flow in axial flow turbines-part III: tip cooling," *Journal of Turbomachinery*, vol. 131, no. 1, pp. 1–12, 2009.

[3] J. S. Park, D. H. Lee, D. H. Rhee, S. H. Kang, and H. H. Cho, "Heat transfer and film cooling effectiveness on the squealer tip of a turbine blade," *Energy*, vol. 72, pp. 331–343, 2014.

[4] J. Ahn, S. Mhetras, and J. C. Han, "Film-cooling effectiveness on a gas turbine blade tip using pressure-sensitive paint," *Journal of Heat Transfer*, vol. 127, no. 5, pp. 521–530, 2005.

[5] Z. Gao, D. Narzary, S. Mhetras, and J. C. Han, "Effect of inlet flow angle on gas turbine blade tip film cooling," *Journal of Turbomachinery*, vol. 131, no. 3, pp. 1–12, 2009.

[6] K. He, "Investigations of film cooling and heat transfer on a turbine blade squealer tip," *Applied Thermal Engineering*, vol. 110, pp. 630–647, 2017.

[7] J. S. Kwak and J. C. Han, "Heat transfer coefficients and film cooling effectiveness on the squealer tip of a gas turbine blade," *Journal of Turbomachinery*, vol. 125, no. 4, pp. 648–657, 2003.

[8] S. Mhetras, D. Narzary, Z. Gao, and J. C. Han, "Effect of a cutback squealer and cavity depth on film-cooling effectiveness on a gas turbine blade tip," *Journal of Turbomachinery*, vol. 130, no. 2, pp. 1–13, 2008.

[9] H. Nasir, S. V. Ekkad, and R. S. Bunker, "Effect of tip and pressure side coolant injection on heat transfer distributions for a plane and recessed tip," *Journal of Turbomachinery*, vol. 129, no. 1, pp. 151–163, 2007.

[10] M. Rezasoltani, K. Lu, M. T. Schobeiri, and J. C. Han, "A combined experimental and numerical study of the turbine blade tip film cooling effectiveness under rotation condition," *Journal of Turbomachinery*, vol. 137, no. 5, pp. 1–12, 2015.

[11] O. Tamunobere and S. Acharya, "Turbine blade tip film cooling with blade rotation-part I: tip and pressure side coolant injection," *Journal of Turbomachinery*, vol. 138, no. 9, pp. 1–8, 2016.

[12] X. Yan, Y. Huang, and K. He, "Investigations into heat transfer and film cooling effect on a squealer- winglet blade tip," *International Journal of Heat and Mass Transfer*, vol. 115, pp. 955–978, 2017.

[13] H. Yang, H. C. Chen, and J. C. Han, "Film-cooling prediction on turbine blade tip with various film hole configurations," *Journal of Thermophysics and Heat Transfer*, vol. 20, no. 3, pp. 558–568, 2006.

[14] A. Arisi, J. Phillips, W. F. Ng, S. Xue, H. K. Moon, and L. Zhang, "An experimental and numerical study on the aerothermal characteristics of a ribbed transonic squealer-tip

turbine blade with purge flow," *Journal of Turbomachinery*, vol. 138, no. 10, pp. 1–11, 2016.

[15] J. Kim, Y. S. Kang, D. Kim, J. Lee, B. J. Cha, and J. Cho, "Optimization of a high pressure turbine blade tip cavity with conjugate heat transfer analysis," *Journal of Mechanical Science and Technology*, vol. 30, no. 12, pp. 5529–5538, 2016.

[16] H. Ma, Q. Zhang, L. He, Z. Wang, and L. Wang, "Cooling injection effect on a transonic squealer tip- part I: experimental heat transfer results and CFD validation," *Journal of Engineering for Gas Turbines and Power*, vol. 139, no. 5, pp. 1–9, 2017.

[17] H. Ma, Q. Zhang, L. He, Z. Wang, and L. Wang, "Cooling injection effect on a transonic squealer tip - part II: analysis of aerothermal interaction physics," *Journal of Engineering for Gas Turbines and Power*, vol. 139, no. 5, pp. 1–9, 2017.

[18] F. Tong, W. Gou, L. Li, Q. Liu, Z. Yue, and G. Xie, "Investigation on heat transfer of a rotor blade tip with various film cooling holes arrangements and groove depths," *Advances in Mechanical Engineering*, vol. 7, no. 2, 2015.

[19] C. Zhou, "Thermal performance of transonic cooled tips in a turbine cascade," *Journal of Guidance, Control, and Dynamics*, vol. 31, no. 5, pp. 1268–1280, 2015.

[20] V. Saxena and S. V. Ekkad, "Effect of squealer geometry on tip flow and heat transfer for a turbine blade in a low speed cascade," *Journal of Heat Transfer*, vol. 126, no. 4, pp. 546–553, 2004.

[21] M. Bang, S. M. Choi, H. S. Sohn, J. S. Park, and H. H. Cho, "Effects of unsteady wakes on heat transfer of blade tip and shroud," *International Communications in Heat and Mass Transfer*, vol. 97, pp. 125–135, 2018.

[22] T. Wang, Y. Xuan, and X. Han, "The effects of tip gap variation on transonic turbine blade tip leakage flow based on VLES approach," *Aerospace Science and Technology*, vol. 111, article 106542, 2021.

[23] K. Zhou and C. Zhou, "Effects of upstream Rankine vortex on tip leakage vortex breakdown in a subsonic turbine," *Aerospace Science and Technology*, vol. 99, article 105776, 2020.

[24] S. Jiang, F. Chen, J. Yu, S. Chen, and Y. Song, "Treatment and optimization of casing and blade tip for aerodynamic control of tip leakage flow in a turbine cascade," *Aerospace Science and Technology*, vol. 86, pp. 704–713, 2019.

[25] T. H. Nguyen, P. Nguyen, and G. F. Tri, "Evaluation of the relationship between the aerothermodynamic process and operational parameters in the high-pressure turbine of an aircraft engine," *Aerospace Science and Technology*, vol. 86, pp. 93–105, 2019.

[26] N. L. Key and T. Arts, "Comparison of turbine tip leakage flow for flat tip and squealer tip geometries at high speed conditions," *ASME Journal of Turbomachinery*, vol. 128, no. 2, pp. 213–220, 2006.

[27] M. Sampson, A. Fairbanks, J. Moseley, P. M. Ligrani, H. Xu, and M. Fox, "Linear Cascade and Wind Tunnel Development for Turbine Blade Tip Heat Transfer Investigations with and without Film Cooling," *Turbo Expo: Power for Land, Sea, and Air*, vol. 58646, 2019.

[28] H. Collopy, P. M. Ligrani, H. Xu, and M. Fox, "Effects of tip gap on transonic turbine blade heat transfer characteristics with pressure side film cooling," *International Journal of Heat and Mass Transfer*, vol. 187, article 122513, 2022.

[29] J. Chappell, P. Ligrani, S. Sreekanth, T. Lucas, and E. Vlasic, "Aerodynamic performance of suction-side gill region film cooling," *Journal of Turbomachinery*, vol. 132, 2010.

[30] R. J. Moffat, "Describing the uncertainties in experimental results," *Experimental Thermal and Fluid Science*, vol. 1, no. 1, pp. 3–17, 1988.

[31] A. S. Virdi, Q. Zhang, L. He, H. D. Li, and R. Hunsley, "Aerothermal performance of shroudless turbine blade tips with relative casing movement effects," *Journal of Propulsion and Power*, vol. 31, no. 2, pp. 527–536, 2015.

[32] D. Narzary, K. Liu, J. C. Han, S. Mhetras, and K. Landis, "Turbine blade tip film-cooling and heat transfer measurements at high blowing ratios," *Turbo Expo: Power for Land, Sea, and Air*, vol. 45721, 2014.

[33] I. Ullah, S. M. Alsaleem, L. M. Wright, C. C. Shiau, and J. C. Han, "Influence of coolant density on turbine blade film cooling at transonic cascade flow conditions using the pressure sensitive paint technique," *Journal of Thermal Science and Engineering Applications*, vol. 14, 2021.